Supporting Information:

Efficient and Stable Deep Blue Thermally Activated Delayed Fluorescence Molecules Based on a Bipyridine Acceptor Core

Cong Cheng,[a] Yongshi Jiang,[a] Haonan Wang,[a] Weiwei Lou,[b] Yunhui Zhu,[a]*
Chao Deng,[a] Dan Wang,[a] Taiju Tsuboi,[a] Guijie Li,[b] Qisheng Zhang[ac]*

[a] MOE Key Laboratory of Macromolecular Synthesis and Functionalization, Department of Polymer Science and Engineering, Zhejiang University, Hangzhou 310027, China.

[b] State Key Laboratory Breeding Base of Green Chemistry-Synthesis Technology, College of Chemical Engineering, Zhejiang University of Technology, Hangzhou 310014, China

[c] State Key laboratory of Clean Energy Utilization, Zhejiang University, Hangzhou 310027, China.

* E-mail: qishengzhang@zju.edu.cn; zhuyh-zdu@zju.edu.cn

Contents

1. Supplemental Tables and Figures

Compound	S_0 state		S_1 state	
	HOMO	LUMO	hole	electron
4Cz2Py	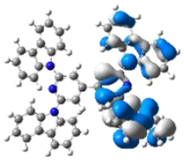	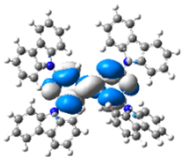	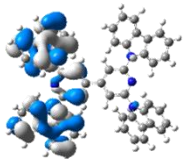	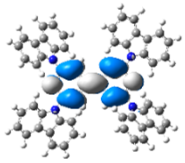
4MeCz2Py	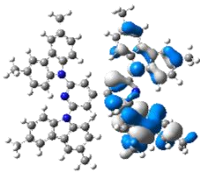	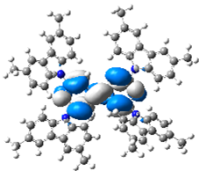	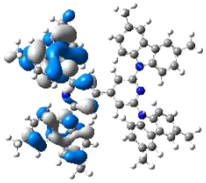	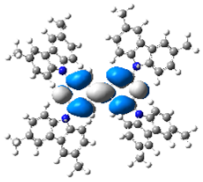
4Cz2Pm	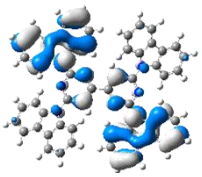	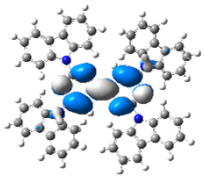	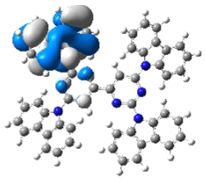	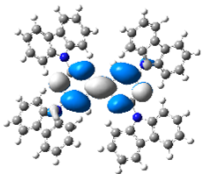
DCzTrz	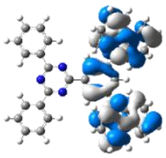	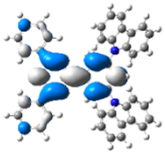	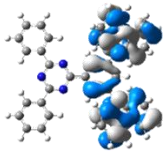	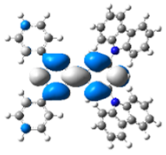
DDCzTrz	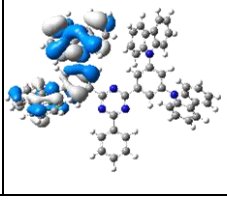	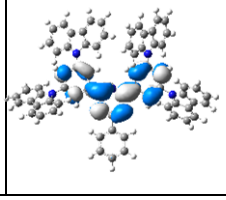	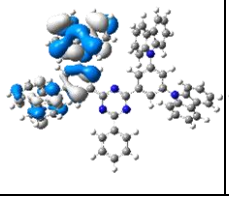	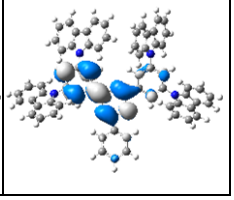

Figure S1. HOMO and LUMO distribution of the compounds in their S_0 state, and electron and hole distribution of the compounds in their S_1 state. The S_0 and S_1 geometries were optimized at the DFT/B3LYP/6-31G* and TDDFT/BMK/6-31G* levels, respectively.

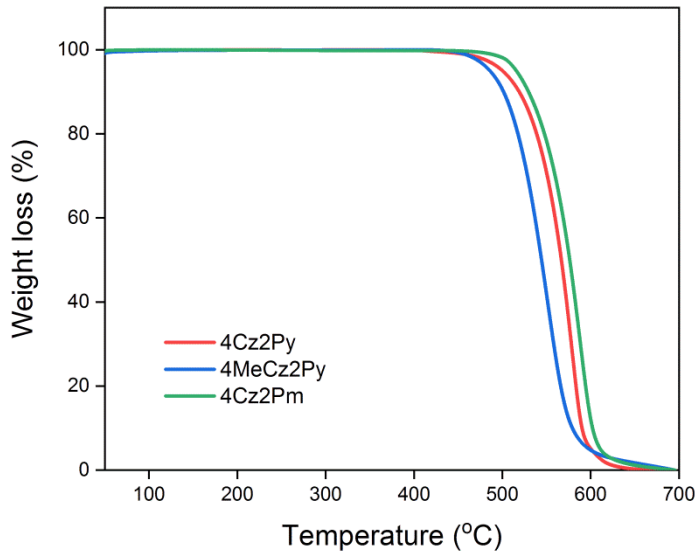

Figure S2. Thermogravimetric analysis of 4Cz2Py, 4MeCz2Py and 4Cz2Pm.

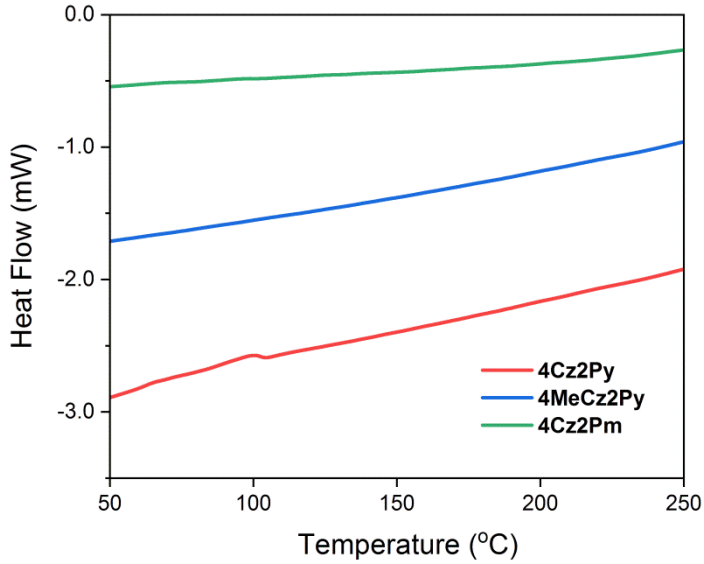

Figure S3. Differential scanning calorimetry of 4Cz2Py, 4MeCz2Py and 4Cz2Pm. No thermal evidence of a glass transition was found in 4MeCz2Py and 4Cz2Pm.

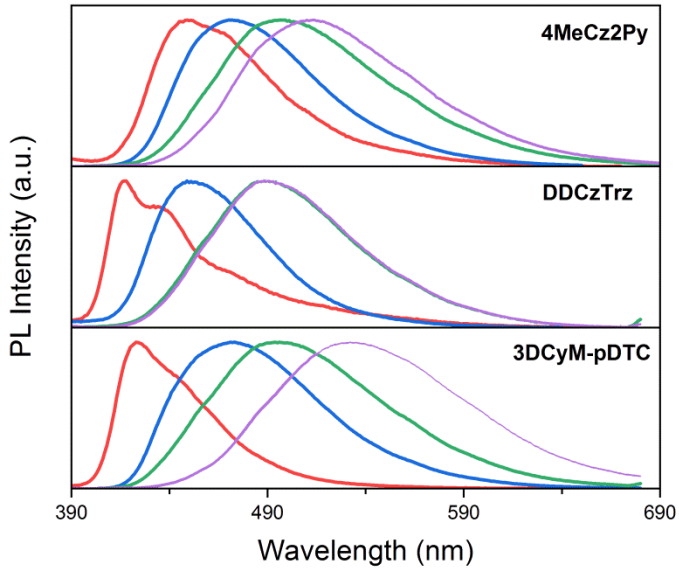

Figure S4. Emission spectra of 4MeCz2Py, DDCzTrz and 3DCyM-pDTC in cyclohexane (red), toluene (blue), tetrahydrofuran (green) and dichloromethane (violet) at RT.

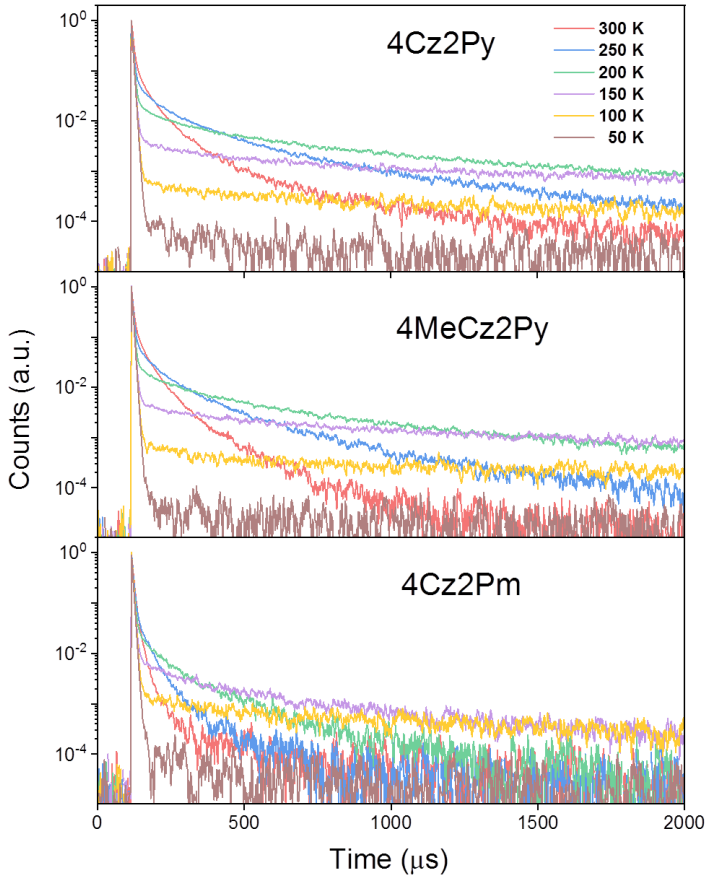

Figure S5. Temperature dependent transient decay spectra of the investigated compounds in 30 wt%-doped PPT films.

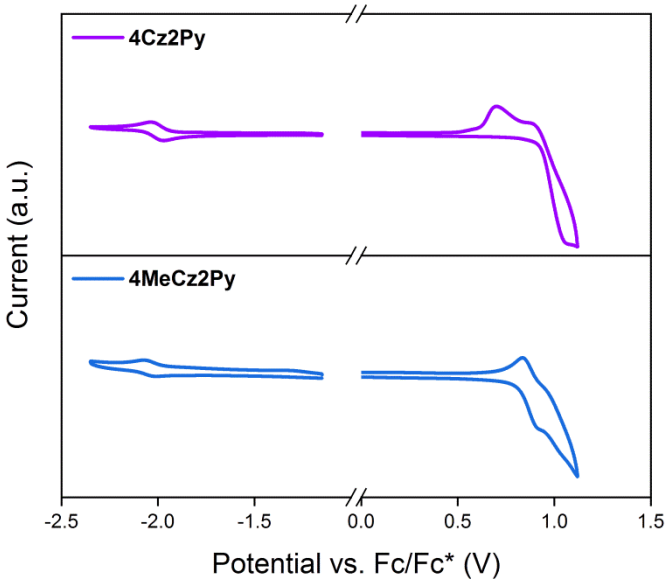

Figure S6. Cyclic voltammograms for the oxidation and reduction processes in dichloromethane and *N*,*N*′-dimethylformamide (DMF), respectively.

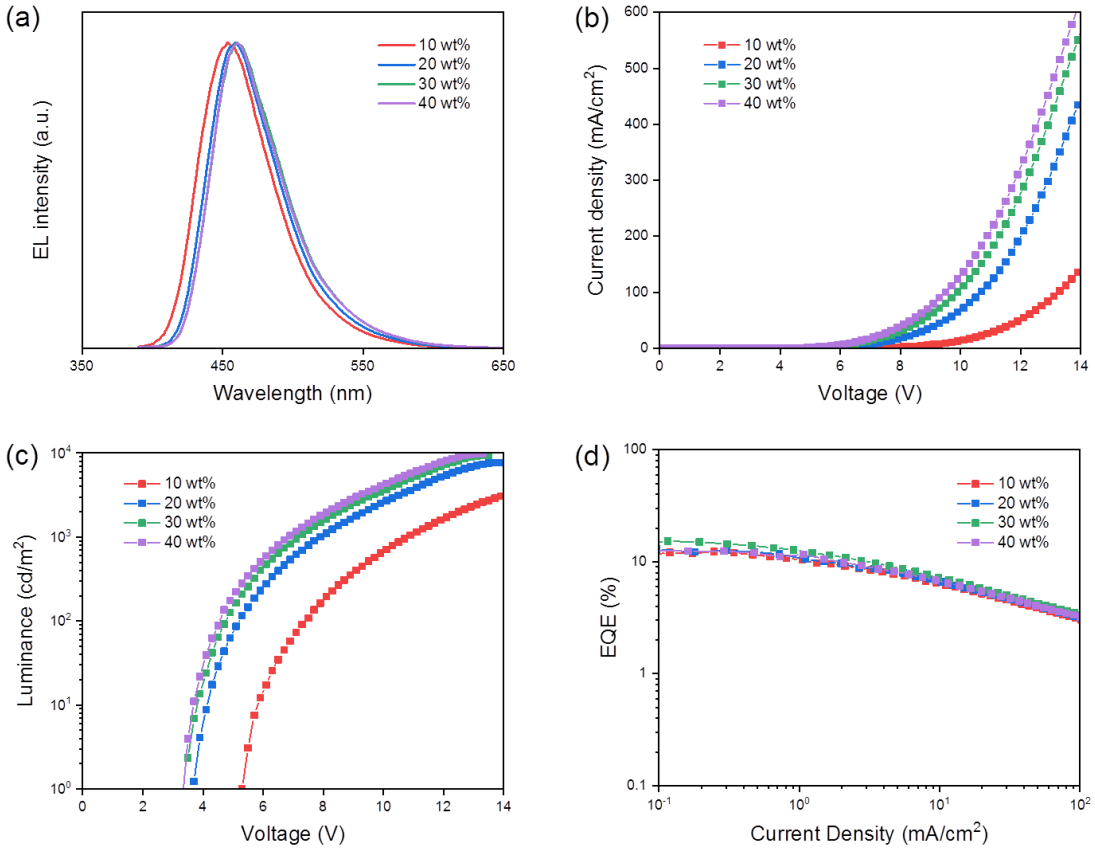

Figure S7. EL spectra (**a**, at 10 mA cm^{-2}), current density–voltage characteristics (**b**), luminance–voltage characteristics (**c**), and EQE–current density characteristics (**d**) of the 4Cz2Py-based OLEDs with different doping concentrations. The device structure (I) is noted in Table 2.

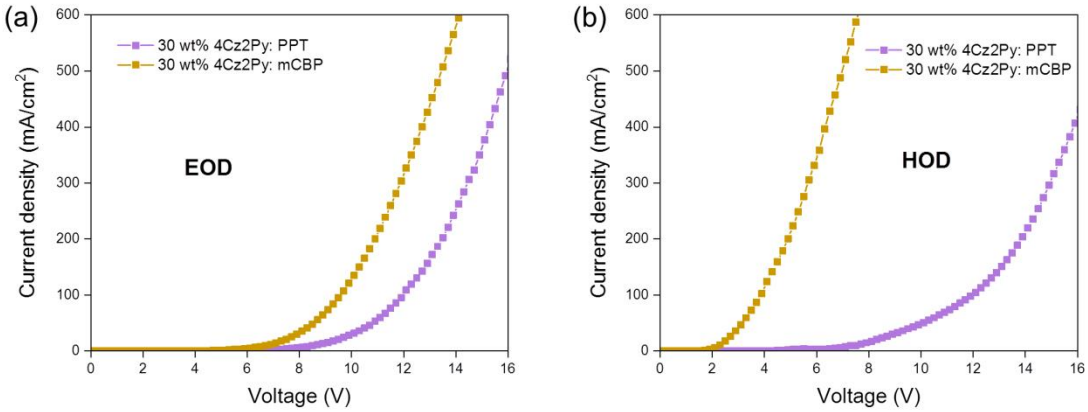

Figure S8. Current density–voltage characteristics of the electron-only (EODs) and hole-only devices (HODs) with structures of ITO/Liq (2 nm)/30 wt% 4Cz2Py: host (60 nm)/$Bepp_2$ (3 nm)/Liq (2 nm)/Al and ITO/MoO_3 (5 nm)/30 wt% 4Cz2Py: host (60 nm)/MoO_3 (5 nm)/Al, respectively.

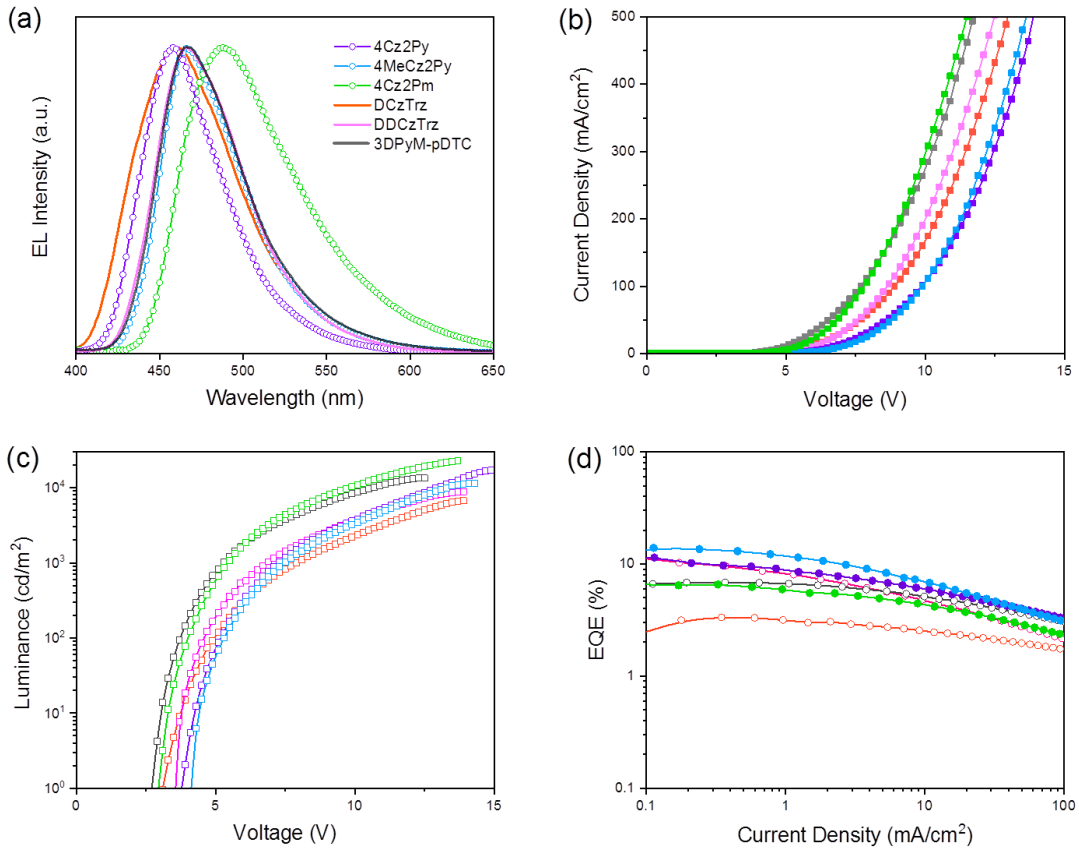

Figure S9. EL spectra (**a**, at 10 mA cm^{-2}), current density–voltage characteristics (**b**), luminance–voltage characteristics (**c**), and EQE–current density characteristics (**d**) of the devices based on different emitters. The device structure (II) is noted in Table 2.

Table S1. Computed twisting angles of the investigated compounds at ground state (DFT/B3LYP/6-31G*) and excited state (TDDFT/BMK/6-31G*).

Compound	Twisting angles in S_0			Twisting angles in S_1		
4Cz2Py	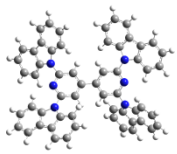	54.22°	31.24°	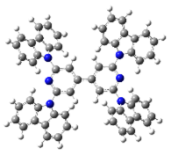	56.01°	40.57°
		32.15°	55.11°		43.68°	59.63°
4MeCz2Py	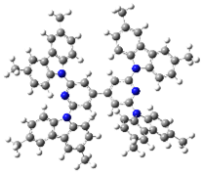	52.40°	29.47°		57.59°	38.61°
		30.60°	53.49°		42.50°	57.83°
4Cz2Pm	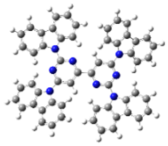	21.50°	33.30°	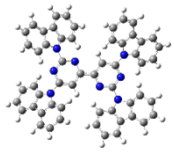	40.96°	37.87°
		33.30°	21.50°		41.79°	23.65°
DCzTrz	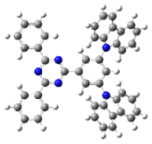	–	55.34°	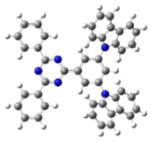	–	50.77°
		–	55.36°		–	51.90°
DDCzTrz	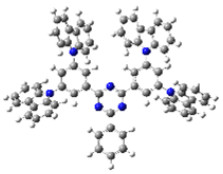	56.86°	48.82°	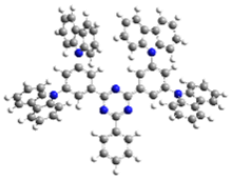	58.13°	46.39°
		53.53°	59.76°		52.78°	53.66°

Table S2. Computed transition energies and oscillator strengths of the investigated molecules on S_0 and S_1 geometries optimized at the DFT/B3LYP/6-31G* level in vacuum and the TDDFT/BMK/6-31G* level in toluene, respectively. All transitions were reproduced by TDDFT/MPW1B95/6-31G* in toluene.

compound	S_0 state				S_1 state				
	S_1 (eV)	T_1 (eV)	ΔE_{ST} (eV)	f	S_1 (eV)	T_1 (eV)	ΔE_{ST} (eV)	f	μ (D)
4Cz2Py	3.2743	2.9890	0.2853	0.0291	2.4777	2.2744	0.2033	0.0300	14.9
4MeCz2Py	3.2117	2.9360	0.2757	0.0363	2.3791	2.2007	0.1784	0.0332	14.7
4Cz2Pm	3.1322	2.8029	0.3293	0.0008	2.1371	2.0125	0.1246	0.0097	18.6
DCzTrz	3.1533	2.9780	0.1753	0.0221	2.7499	2.5417	0.2082	0.0265	13.6
DDCzTrz	3.0146	2.8328	0.1818	0.0199	2.5895	2.3818	0.2077	0.0230	15.0

Table S3. Performances of reported deep blue TADF OLEDs.

Emitter	CIE	EQE_{max} (%)	Ref.
DTC-DPS	0.15, 0.07	9.9	1
DTC-mBPSB	0.15, 0.08	5.5	2
CzBPCN	0.14, 0.12	14.0	3
BPy-pC	0.16, 0.13	4.2	4
SPXZPO	0.16, 0.12	6.3	5
3b	0.16, 0.08	8.5	6
ICzAc	0.15, 0.09	13.7	7
BDTPDDA	0.14, 0.12	8.5	8
2CzdOXDMe	0.16, 0.12	4.7	9
2CzdOXD4MeOPh	0.15, 0.11	6.6	9
DCzBN3	0.16, 0.06	10.3	10
DtBuAc-DBT	0.13, 0.13	10.5	11
PXB-mIC	0.15, 0.08	12.5	12
tCz-ND	0.14, 0.16	17.0	13
4Cz2Py	0.14, 0.12	15.1	this work

2. Experimental Section

2.1 Materials and measurement:

All solvents and starting materials were purchased from commercial resources and were used as received unless otherwise stated. OLED materials for device

fabrication were purchased from Jilin optical and electronic materials Co. Ltd and were used without further purification. 9,9'-(5-(4,6-diphenyl-1,3,5-triazin-2-yl)-1,3-phenylene)bis(9H-carbazole) (DCzTrz) and 9,9',9",9'"-((6-phenyl-1,3,5-triazine-2,4-diyl)bis(benzene-5,3,1-triyl))tetrakis(9H-carbazole) (DDCzTrz) and bis(5-(3,6-di-tert-butyl-9H-carbazol-9-yl)pyridin-2-yl)methanone (3DPyM-pDTC) were synthesized according to previous reports.[14, 15] Nuclear magnetic resonance (NMR) spectroscopy were recorded on a Bruker Avance III 400 spectrometer (^{1}H: 400 MHz and ^{13}C: 100 MHz) at room temperature using $CDCl_3$ as the solvent and tetramethylsilane (TMS) as the internal reference. MALDI-TOF mass spectra were performed on an AXIMA CFR MS apparatus (COMPACT). Accurate mass determination was corrected by calibration using the sodium trifluoroacetate clusters as reference. Elemental analyses (C, H, N) were carried out with a Vario MICRO cube (Elementar). Thermogravimetric analysis (TGA) and differential scanning calorimetry (DSC) were tested using TA Q500 and TA Q200, respectively. The TGA curve was measured at heating rate of 10 °C/min from room temperature to 800 °C under nitrogen flow. The DSC curve was measured at heating rate of 10 °C/min from room temperature to 300 °C under nitrogen flow.

2.2 Synthesis:

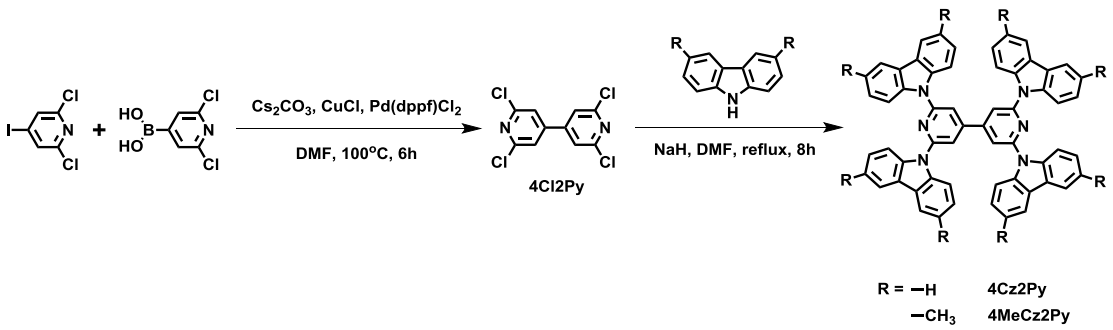

Scheme S1. Synthesis route of **4Cz2Py** and **4MeCz2Py**

2,6,2′,6′-Tetrachloro-4,4′-bipyridine (4Cl2Py):

A mixture of 2,6-dichloro-4-iodopyridine (0.55 g, 2.0 mmol), (2,6-dichloropyridin-4-yl)boronic acid (0.46 g, 2.4 mmol), Cs_2CO_3 (2.6 g, 8.0 mmol),

$Pd(dppf)Cl_2$ (0.073 g, 0.1 mmol, 5 mol %) and CuCl (0.79 g, 8.0 mmol) in 20 mL DMF was heated at 100 ℃ for 6 h under a nitrogen flow. The reaction mixture was cooled and then the solvent was evaporated under a reduced pressure. The residue was purified by column chromatography (Vol. DCM/PE=1/5) to afford **4Cl2Py** 0.26 g (45% yield) as a white powder. ^{1}H NMR (400 MHz, $CDCl_3$): δ 7.46 (s, 4H) [ppm].

2,6,2′,6′-Tetra(9H-carbazol-9-yl)-4,4′-bipyridine (4Cz2Py):

A mixture of 9H-carbazole (0.42 g, 2.5 mmol) and NaH (0.062 g, 2.6 mmol) was stirred in 20 mL DMF at 0 ℃ for 0.5 h under a nitrogen flow. Then 0.15 g **4Cl2Py** powder (0.5 mmol) was added and the reaction mixture was heated to reflux for 8 h. The reaction mixture was cooled to room temperature and quenched by adding water. The mixture was poured into water and filtered to give the precipitated crude product. The product was dried and then purified by column chromatography (Vol. DCM/PE=1/1) to afford **4Cz2Py** 0.13 g (31% yield) as a yellow-green solid. ^{1}H NMR (400 MHz, $CDCl_3$): δ 8.19-8.16 (m, 16H), 8.00 (s, 4H), 7.46-7.36 (m, 16H). [ppm]; ^{13}C NMR (100 MHz, $CDCl_3$): δ 152.77, 139.34, 126.66, 124.93, 121.80, 120.32, 112.19, 111.89, 77.22 [ppm]. MALDI-TOF $[M]^+$ calcd. for $C_{58}H_{36}N_6$ 816.300, found 816.335. Anal Calcd for $C_{48}H_{52}N_8$: C, 85.27%; H, 4.44%; N, 10.29%. Found: C, 85.27%; H, 4.43%; N, 10.30%.

2,6,2′,6′-Tetra(3,6-dimethylcarbazol-9-yl)-4,4′-bipyridine (4MeCz2Py) was obtained by a method the same as that for 4Cz2Py**.** Yellow-green solid, yield: 0.68 g, 47%. ^{1}H NMR (400 MHz, $CDCl_3$): δ 8.07 (d, J = 8.4 Hz, 8H), 7.91-7.90 (m, 12H), 7.23-7.21 (m, 8H), 2.55 (s, 24H) [ppm]; ^{13}C NMR (100 MHz, $CDCl_3$): δ 137.77, 137.47 131.01, 127.73, 125.03, 120.13, 112.18, 110.65, 77.23, 21.42 [ppm]. MALDI-TOF $[M]^+$ calcd. for $C_{66}H_{52}N_6$ 928.425, found 928.584. Anal Calcd for $C_{48}H_{52}N_8$: C, 85.31%; H, 5.64%; N, 9.04%. Found: C, 85.30%; H, 5.68%; N, 9.02%.

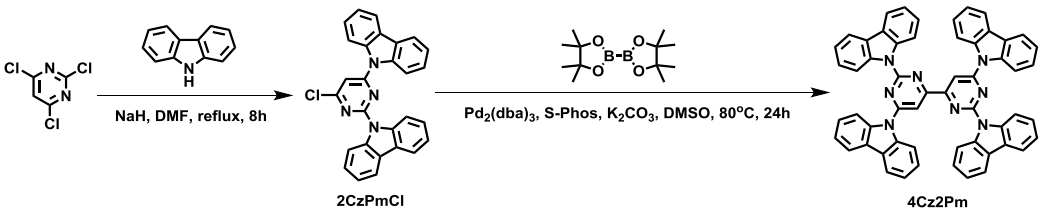

Scheme S2. Synthesis route of **4Cz2Pm**

4-Chloro-2,6-di(9H-carbazol-9-yl)-pyrimidine (2CzPmCl)

The intermediate material was synthesized according to a previous report.[15] A mixture of 9H-carbazole (1.1 g, 6.6 mmol) and NaH (0.16 g, 6.6 mmol) was stirred in 20 mL DMF at 0 ℃ for 0.5 h under a nitrogen flow. Then 2,4,6-trichloropyrimidine 0.55 g (3.0 mmol) was added and the reaction mixture was heated to reflux for 8 h. The reaction mixture was cooled to room temperature and quenched by adding water. The mixture was poured into water and filtered to give the precipitated crude product. The product was dried and then purified by column chromatography (Vol. DCM/PE=1/2) to afford **2CzPmCl** 0.63 g (47% yield) as a white solid. ^{1}H NMR (400 MHz, $CDCl_3$): δ 8.96 (d, *J* = 8.0 Hz, 2H), 8.11 (d, *J* = 8.0 Hz, 2H), 8.07 (d, *J* = 8.0 Hz, 2H), 8.08 (d, *J* = 8.0 Hz, 2H), 7.49-7.44 (m, 5H), 7.42-7.37 (m, 4H) [ppm].

2,2′,6,6′-Tetra(9H-carbazol-9-yl)-4,4′-bipyrimidine (4Cz2Pm)

A mixture of **2CzPmCl** (0.45 g, 1.0 mmol), bis(pinacolato)diboron (0.15 g, 0.6 mmol), K_2CO_3 (0.21 g, 1.5 mmol), $Pd_2(dba)_3$ (0.045 g, 0.05 mmol, 5 mol %) and S-phos (0.041 g, 0.1 mmol, 10 mol%) in 20 mL DMSO was heated at 80 ℃ for 24 h under a nitrogen flow. The reaction mixture was cooled and poured into water, then filtered to give an insoluble product. The residue was purified by sublimation to afford **4Cz2Pm** 0.25 g (61% yield) as a yellow solid. ^{1}H NMR and ^{13}C NMR could not obtained because of its insolubility. MALDI-TOF $[M+H]^+$ calcd. for $C_{56}H_{34}N_8$ 819.291, found 819.300. Anal Calcd for $C_{48}H_{52}N_8$: C, 82.13%; H, 4.18%; N, 13.68%. Found: C, 82.16%; H, 4.17%; N, 13.67%.

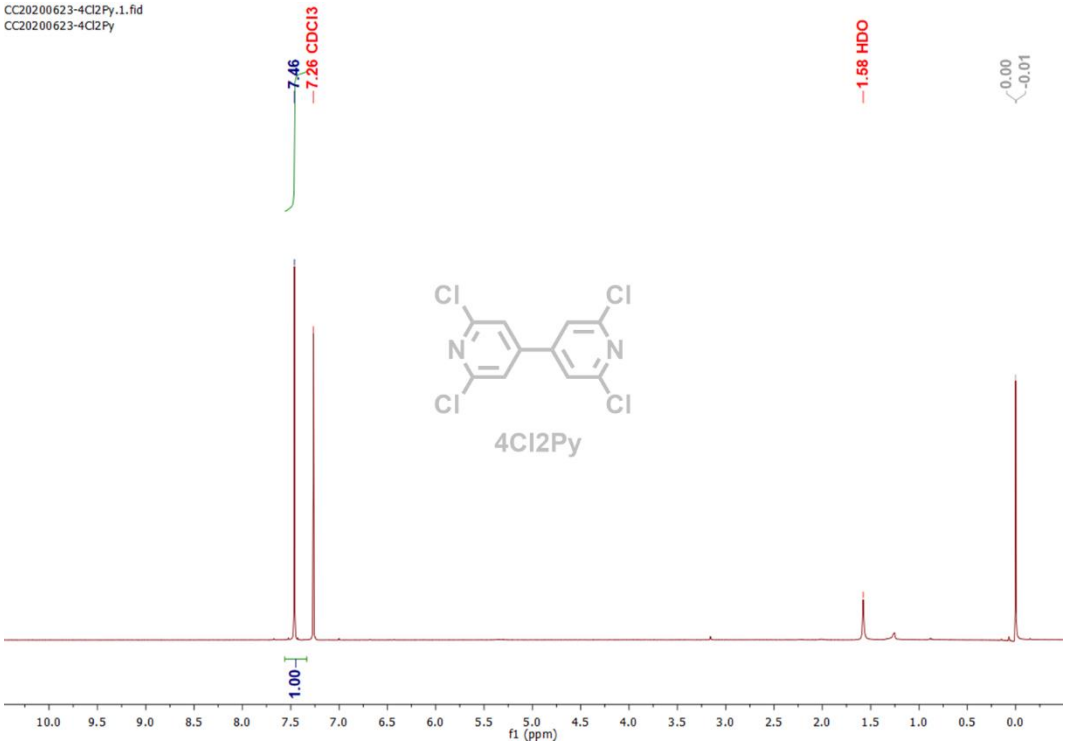

Figure S9. ^{1}H NMR spectra of **4Cl2Py**.

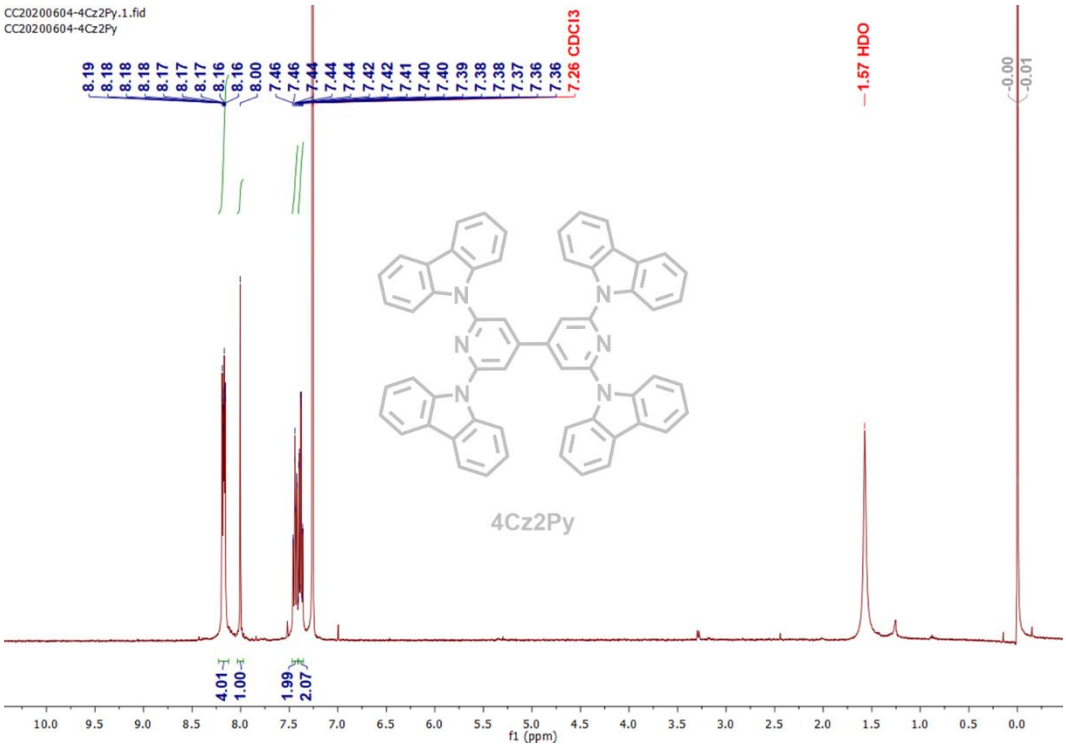

Figure S10. ^{1}H NMR spectra of **4Cz2Py**.

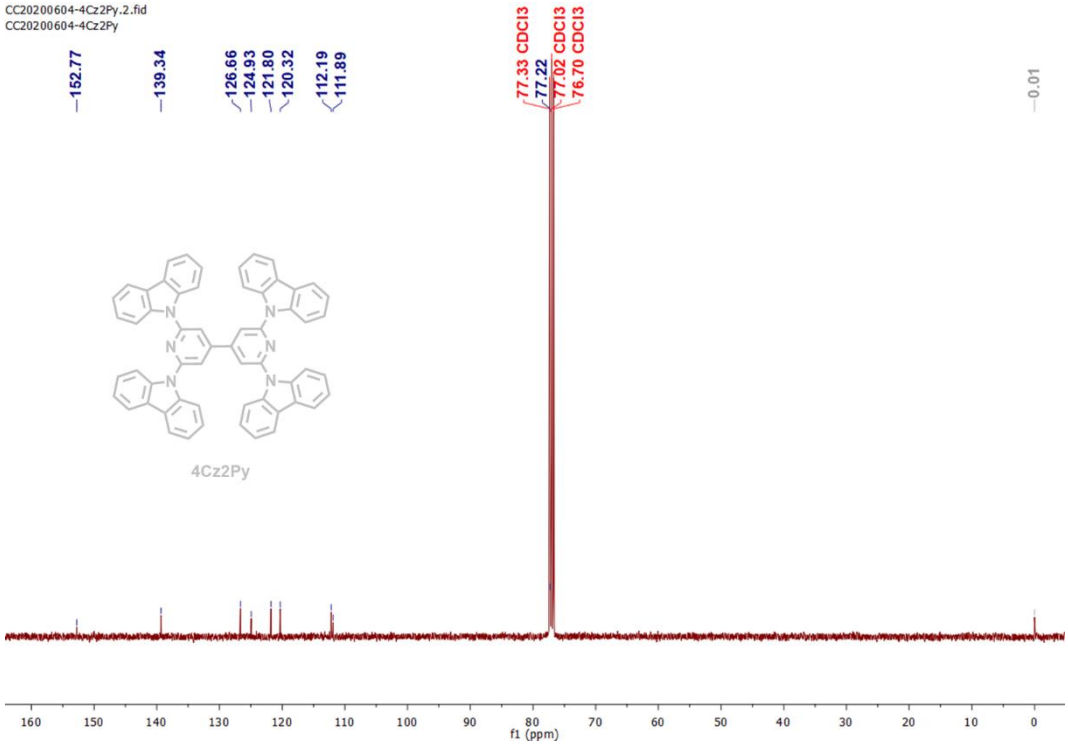

Figure S11. ^{13}C NMR spectra of **4Cz2Py**.

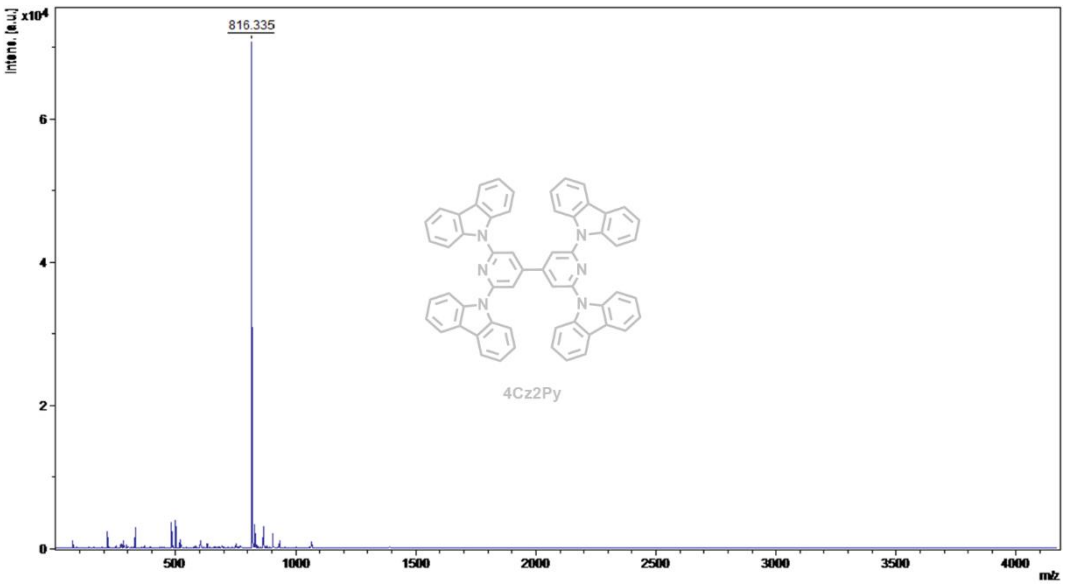

Figure S12. MALDI-TOF-MS spectrum of **4Cz2Py**.

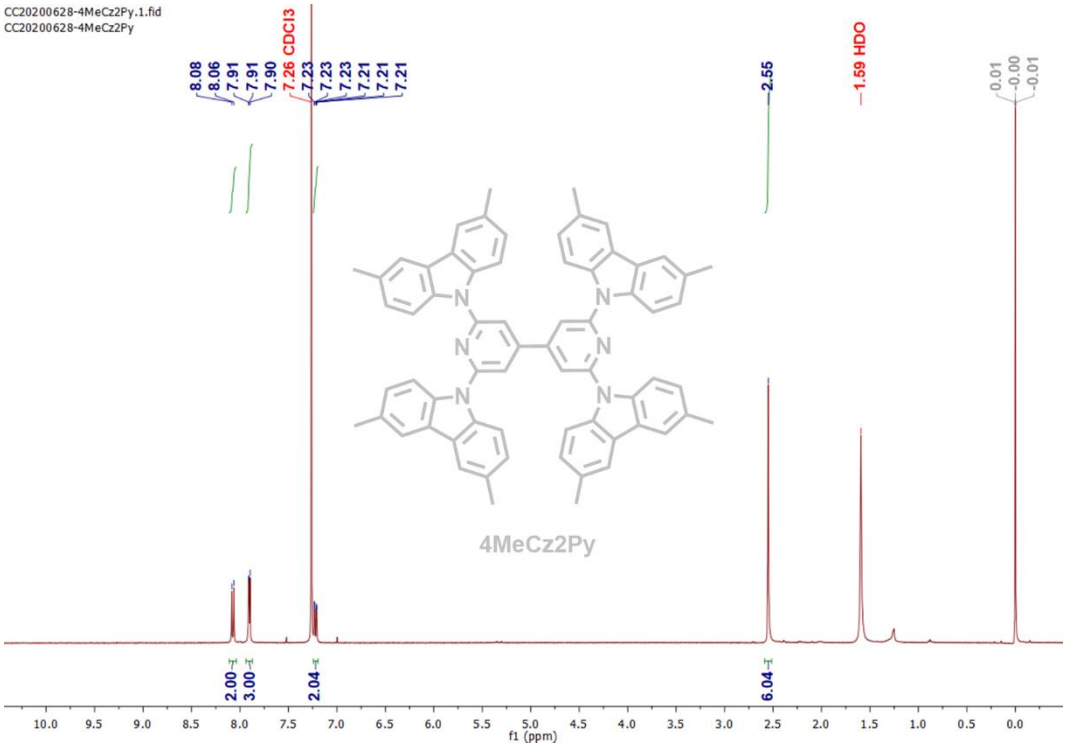

Figure S13. ^{1}H NMR spectra of **4MeCz2Py**.

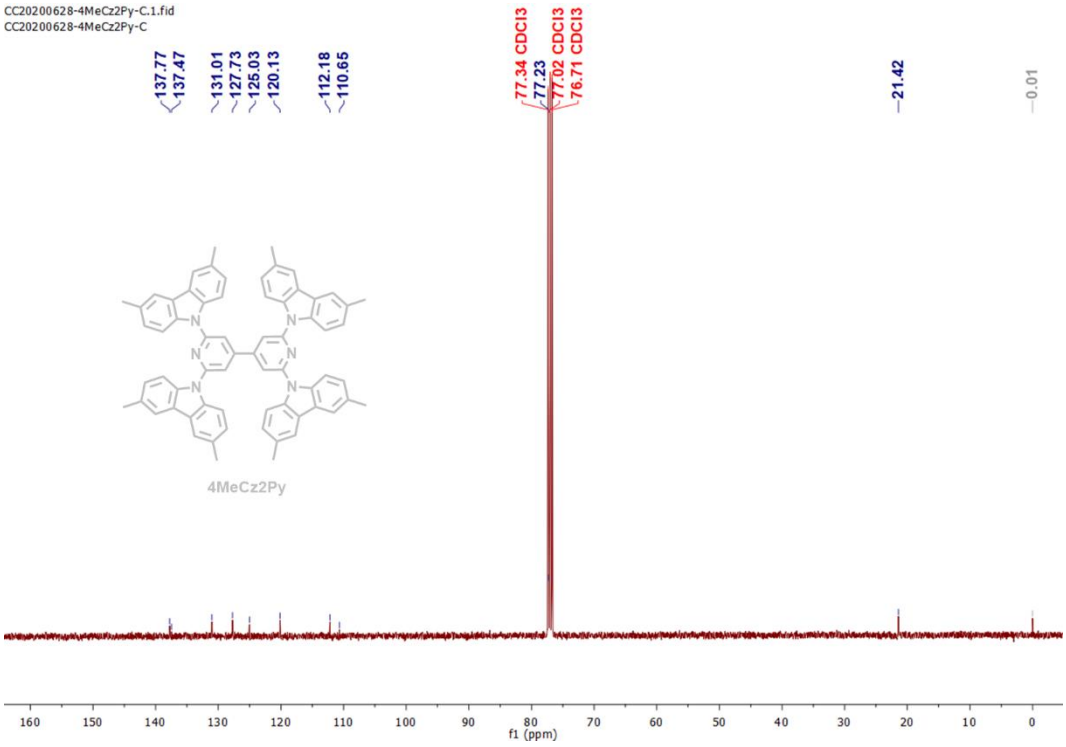

Figure S14. ^{13}C NMR spectra of **4MeCz2Py**.

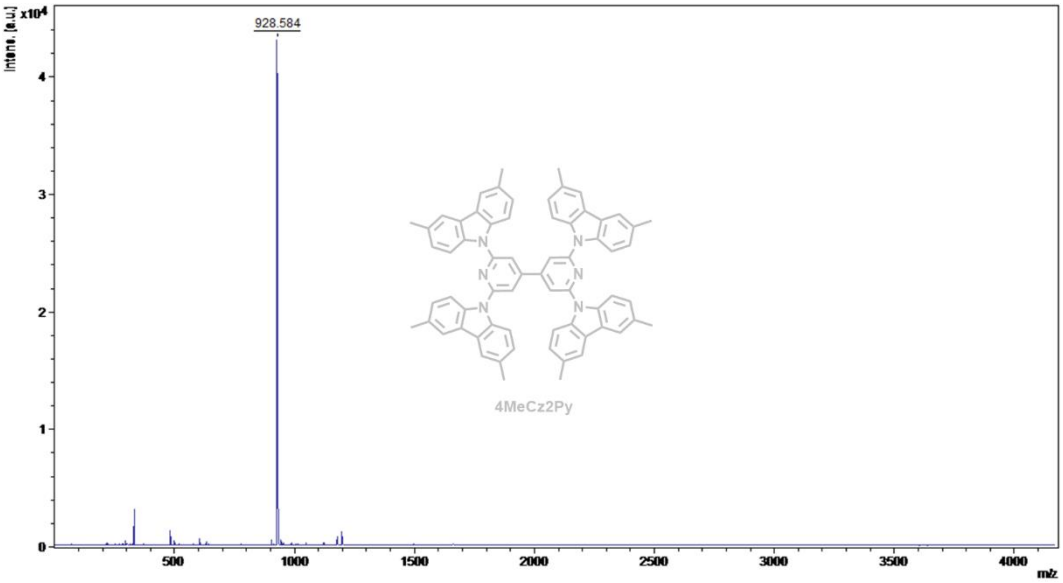

Figure S15. MALDI-TOF-MS spectrum of **4MeCz2Py**.

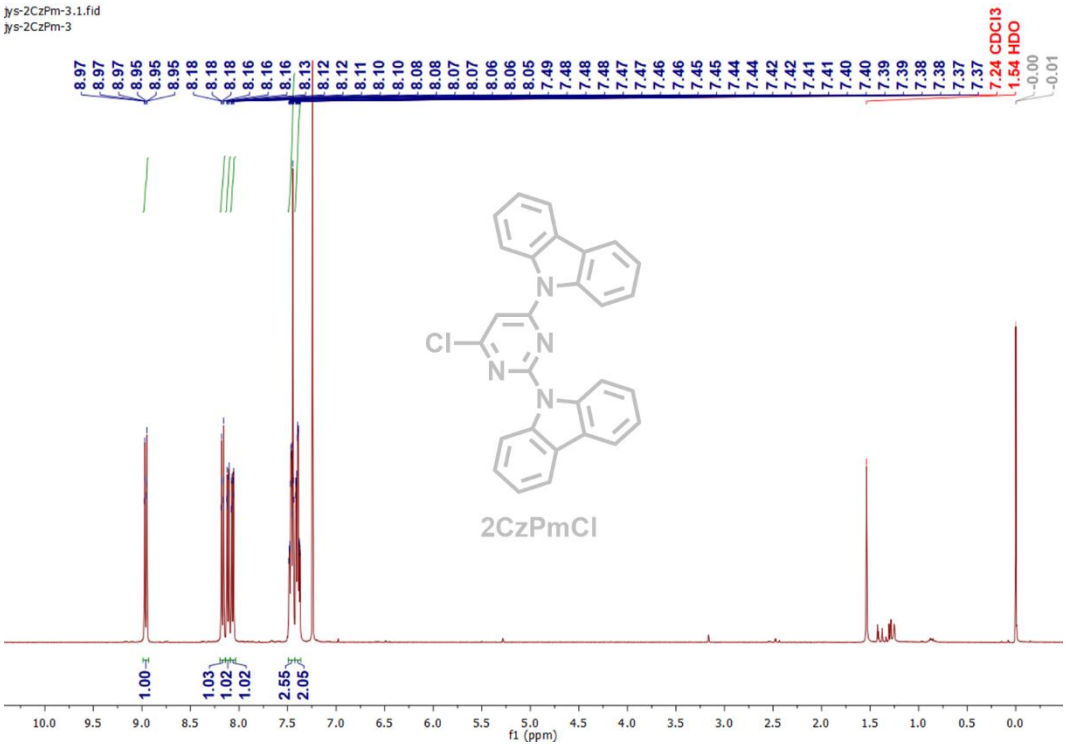

Figure S16. ^{1}H NMR spectra of **2CzPmCl**.

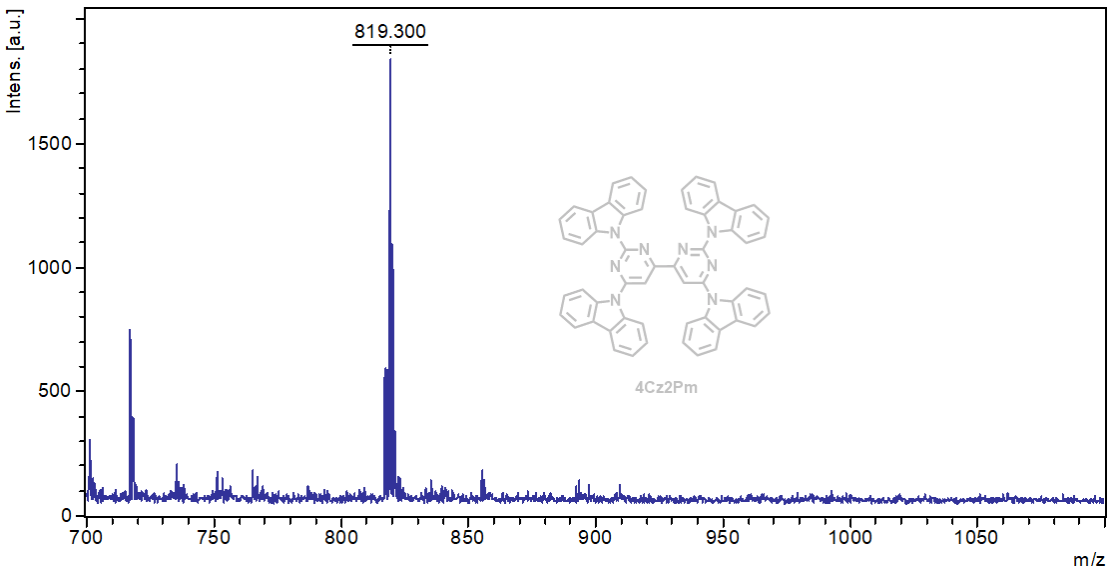

Figure S17. MALDI-TOF-MS spectrum of **4Cz2Pm**.

2.3 Photoluminescence (PL) measurements:

UV-VIS absorption was measured using a Shimadzu UV2600 UV/VIS spectrophotometer. The photoluminescence (PL) spectra and quantum yield of the samples were measured using a QM-40 spectrofluorometer (PTI, Horiba) equipped with a 150 W xenon lamp and an integrating sphere. The transient fluorescence decay spectra were recorded on Horiba DeltaFlex modular lifetime measurement system patented TCSPC technique, equipped with a diode laser as excitation source (λ = 370 nm, pulse width ≈ 50 ps, repetition rate = 20.00 kHz). The time-resolved emission spectra of fluorescence (1 ns delay) and phosphorescence (1 ms delay) at 77 K were recorded by a PTI TimeMaster fluorimeter equipped with a PTI nitrogen laser (GL-3300, λ = 266 nm, pulse width ≈ 1 ns, pulse energy = 1.45 mJ).

2.4 Electrochemical measurements:

Cyclic voltammetry was performed using a CHI 600E electrochemical analyzer S-20 in a gas-tight three-electrode cell at room temperature. A glassy carbon working electrode (Φ = 5.0 mm), a platinum wire auxiliary electrode, and an Ag/Ag^+ reference electrodes (0.1 M $AgNO_3$, 0.1 M tetrabutylammonium hexafluorophosphate (TBAP) in acetonitrile) were used. The oxidation and reduction processes were measured by

scanning the potential at a scan rate of 100 mV/s in dichloromethane and *N,N′*-dimethylformamide, respectively, with 0.1 M TBAP as supporting electrolyte. The solutions were degassed by purging with N_2 gas for approximately 3 minutes before the measurement. The ferrocene couple Fc^+/Fc was selected as the external reference.

2.5 Quantum chemical calculations:

All calculations were performed using the Gaussian 09 program package.[17] The geometries at ground state were optimized via DFT calculations at the B3LYP/6-31G* level in vacuum, while the geometries in S_1 were optimized via TDDFT calculations at the BMK/6-31G* level in toluene. Frequency analysis was used to confirm that the structures are at the local minima of the potential surfaces. The excitation energy levels and oscillator strengths (*f*) of the $S_0 \rightarrow S_1$ transition were calculated based on TDDFT with the MPW1B95 functionals using 6-31G* basis sets in toluene. Based on the optimized ground state and excited state electronic structures, the overlap integrals of HOMO and LUMO were calculated using Multiwfn 3.5.[18]

2.6 Device fabrication and measurements:

For OLED fabrication, all of the inorganic, organic layers and metal layer were thermally evaporated on the cleaned Indium-tin-oxide (ITO) glass substrate under vacuum ($< 5\times10^{-4}$ Pa). The active area of the devices is 9 mm^2. The deposition rates were 0.1 Å/s for MoO_3 layer, 1-2 Å/s for organic layers, and 4 Å/s for Al layer. The current density, voltage and luminance characteristics of the devices were measured in ambient air with a Keithey 2400 Source meter and a Keithey 2000 Source multimeter equipped with a calibrated silicon photodiode. The electroluminescence spectra were recorded using a multichannel spectrometer (PMA12, Hamamatsu Photonics). Assuming Lambertian emission, the external quantum efficiency can be calculated from the luminance, current density, and EL spectrum. The operational lifetimes of encapsulated OLEDs were performed with a multi-channel OLED Lifetime Test System designed by Prof. Zhilin Zhang at Shanghai University.

3. References

[1] Zhang, Q.; Li, J.; Shizu, K.; Huang, S.; Hirata, S.; Miyazaki, H.; Adachi, C. Design of Efficient Thermally Activated Delayed Fluorescence Materials for Pure Blue Organic Light Emitting Diodes. *J. Am. Chem. Soc.* **2012,** *134,* 14706−14709.

[2] Liu, M.; Seino, Y.; Chen, D.; Inomata, S.; Su, S. J.; Sasabe, H.; Kido, J. Blue Thermally Activated Delayed Fluorescence Materials Based on Bis(Phenylsulfonyl)Benzene Derivatives. *Chem. Commun.* **2015,** *51,* 16353−16356.

[3] Cho, Y. J.; Jeon, S. K.; Lee, S. S.; Yu, E.; Lee, J. Y. Donor Interlocked Molecular Design for Fluorescence-Like Narrow Emissioin Deep Blue Thermally Activated Delayed Fluorescent Emitters. *Chem. Mater.* **2016,** *28,* 5400−5405.

[4] Rajamalli, P.; Senthilkumar, N.; Gandeepan, P.; Ren-Wu, C. C.; Lin, H. W.; Cheng, C. H. A Method for Reducing the Singlet-Triplet Energy Gaps of TADF Materials for Improving the Blue OLED Efficiency. *ACS Appl. Mater. Interfaces* **2016,** *8,* 27026−27034.

[5] Duan, C. B.; Li, J.; Han, C. M.; Ding, D. X.; Yang, H.; Wei, Y.; Xu, H. Multi-dipolar Chromophores Featuring Phosphine Oxide as Joint Acceptor: A New Strategy toward High-Efficiency Blue Thermally Activated Delayed Fluorescence Dyes. *Chem. Mater.* **2016,** *28,* 5667−5679.

[6] Jurgensen, N.; Kretzschrnar, A.; Hofle, S.; Freudenberg, J.; Bunz, U. H. F.; Hernandez-Sosa, G. Sulfone-Based Deep Blue Thermally Activated Delayed Fluorescence Emitters: Solution-Processed Organic Light-Emitting Diodes with High Efficiency and Brightness. *Chem. Mater.* **2017,** *29,* 9154−9161.

[7] Seo, J. A.; Im, Y.; Han, S. H.; Lee, C. W.; Lee, J. Y. Unconventional Molecular Design Approach of High-Efficiency Deep Blue Thermally Activated Delayed Fluorescent Emitters Using Indolocarbazole as an Acceptor. *ACS Appl. Mater. Interfaces* **2017,** *9,* 37864−37872.

[8] Woo, S. J.; Kim, Y.; Kim, M. J.; Baek, J. Y.; Kwon, S. K.; Kim, Y. H.; Kim, J. J. Strategies for the Molecular Design of Donor-Acceptor-Type Fluorescent Emitters for Efficient Deep Blue Organic Light Emitting Diodes. *Chem. Mater.* **2018,** *30,* 857−863.

[9] Wong, M. Y.; Krotkus, S.; Copley, G.; Li, W.; Murawski, C.; Hall, D.; Hedley, G. J.; Jaricot, M.; Cordes, D. B.; Slawin, A. M. Z.; Olivier, Y.; Beljonne, D.; Muccioli, L.; Moral, M.; Sancho-Garcia, J. C.; Gather, M. C.; Samuel, I. D. W.; Zysman-Colman, E. Deep-Blue Oxadiazole-Containing Thermally Activated Delayed Fluorescence Emitters for Organic Light-Emitting Diodes. *ACS Appl. Mater. Interfaces* **2018,** *10,* 33360−33372.

[10] Chan, C. Y.; Cui, L. S.; Kim, J. U.; Nakanotani, H.; Adachi, C. Rational Molecular Design for Deep‐Blue Thermally Activated Delayed Fluorescence Emitters. *Adv. Funct. Mater.* **2018,** *28,* 1706023.

[11] Huang, R. J.; Kukhta, N.; Ward, J. S.; Danos, A.; Batsanov, A. S.; Bryce, M. R.; Dias, F. B. Balancing Charge-Transfer Strength and Triplet States for Deep-Blue Thermally Activated Delayed Fluorescence with an Unconventional Electron Rich Dibenzothiophene Acceptor. *J. Mater. Chem. C* **2019,** *7,* 13224−13234.

[12] Ahn, D. H.; Lee, H.; Kim, S. W.; Karthik, D.; Lee, J.; Jeong, H.; Lee, J. Y.; Kwon, J. H. Highly Twisted Donor-Acceptor Boron Emitter and High Triplet Host Material for Highly Efficient Blue Thermally Activated Delayed Fluorescent Device. *ACS Appl. Mater. Interfaces*

2019, *11*, 14909−14916.

[13]Kreiza, G.; Banevicius, D.; Jovais aite, J.; Jursenas, S.; Javorskis, T.; Vaitkevicius, V.; Orentas E.; Kazlauskas, K. Realization of deep-blue TADF in sterically controlled naphthyridines for vacuum- and solution-processed OLEDs. *J. Mater. Chem. C*, **2020**, *8*, 8560−8566.

[14]Kim, M.; Jeon, S. K.; Hwang, S. H.; Lee, J. Y. Stable Blue Thermally Activated Delayed Fluorescent Organic Light-Emitting Diodes With Three Times Longer Lifetime Than Phosphorescent Organic Light-Emitting Diodes. *Adv. Mater.* **2015,** *27*, 2515−2520.

[15]Rajamalli, P.; Senthilkumar, N.; Huang, P. Y.; Ren-Wu, C. C.; Lin, H. W.; Cheng, C. H. New Molecular Design Concurrently Providing Superior Pure Blue, Thermally Activated Delayed Fluorescence and Optical Out-Coupling Efficiencies. *J. Am. Chem. Soc.* **2017,** *139*, 10948−10951.

[16]Li, S. W.; Yu, C. H.; Ko, C. L.; Chatterjee, T.; Hung, W. Y.; Wong, K. T. Cyanopyrimidine-Carbazole Hybrid Host Materials for High-Efficiency and Low-Efficiency Roll-Off TADF OLEDs. *ACS Appl. Mater. Interfaces* **2018**, *10*, 12930−12936.

[17]Frisch, M. J.; Trucks, G. W.; Schlegel, H. B.; Scuseria, G. E.; Robb, M. A.; Cheeseman, J. R.; Scalmani, G.; Barone, V.; Mennucci, B.; Petersson, G. A.; Nakatsuji, H.; Caricato, M.; Li, X.; Hratchian, H. P.; Izmaylov, A. F.; Bloino, J.; Zheng, G.; Sonnenberg, J. L.; Hada, M.; Ehara, M.; Toyota, K.; Fukuda, R.; Hasegawa, J.; Ishida, M.; Nakajima, T.; Honda, Y.; Kitao, O.; Nakai, H.; Vreven, T.; Montgomery, Jr., J. A.; Peralta, J. E.; Ogliaro, F.; Bearpark, M.; Heyd, J. J.; Brothers, E.; Kudin, K. N.; Staroverov, V. N.; Keith, T.; Kobayashi, R.; Normand, J.; Raghavachari, K.; Rendell, A.; Burant, J. C.; Iyengar, S. S.; Tomasi, J.; Cossi, M.; Rega, N.; Millam, J. M.; Klene, M.; Knox, J. E.; Cross, J. B.; Bakken, V.; Adamo, C.; Jaramillo, J.; Gomperts, R.; Stratmann, R. E.; Yazyev, O.; Austin, A. J.; Cammi, R.; Pomelli, C.; Ochterski, J. W.; Martin, R. L.; Morokuma, K.; Zakrzewski, V. G.; Voth, G. A.; Salvador, P.; Dannenberg, J. J.; Dapprich, S.; Daniels, A. D.; Farkas, O.; Foresman, J. B.; Ortiz, J. V.; Cioslowski, J.; Fox, D. J. Gaussion 09, Revision D.01; Gaussian, Inc.: 2009.

[18]Lu, T.; Chen, F. Multiwfn: A Multifunctional Wavefunction Analyzer. *J. Comput. Chem.* **2012**, *33*, 580–592.